Sveriges lantbruksuniversitet
Swedish University of Agricultural Sciences

**Faculty of Veterinary Medicine
and Animal Science**

Using inertial sensors for assessing movement symmetries in trotting dogs

- A feasibility study

Anders Stenman

Uppsala
2019

Degree Project 30 credits within the Veterinary Medicine Programme

Using inertial sensors for assessing movement symmetries in trotting dogs
- A feasibility study

Anders Stenman

Supervisor: *Anna Bergh, Department of Clinical Sciences*

Assistant Supervisor: *Anja Pedersen, Department of Clinical Sciences*

Examiner: *Marie Rhodin, Department of Anatomy, Physiology and Biochemistry*

Degree Project in Veterinary Medicine

Credits: *30*
Level: *Second cycle, A2E*
Course code: *EX0869*

Place of publication: *Uppsala*
Year of publication: *2019*
Online publication: *https://stud.epsilon.slu.se*

Key words: *lameness, lameness assessment, inertial sensors, dogs, trot*
Nyckelord: *hälta, hältbedömning, tröghetssensorer, hundar, trav*

Sveriges lantbruksuniversitet
Swedish University of Agricultural Sciences

Faculty of Veterinary Medicine and Animal Science
Department of Clinical Sciences

SUMMARY

Lameness or other disturbances in the musculoskeletal system are common reasons why dog owners seek veterinary care. The lameness is most often associated with pain, degenerative changes in joints or muscles, or injury.

Evaluation of lameness have traditionally been performed subjectively by means of visual assessment and scoring. Such methods are well established in field of equine medicine where the examiner typically observes the ventro-dorsal movements of the head, the withers and the pelvis during locomotion. A major problem with subjective assessment, however, is that different examiners will arrive at different results. This has been confirmed in studies carried out both within the fields of equine medicine and small animal medicine. Unfortunately, the situation becomes even more challenging when it comes to companion pets such as dogs, as their movements are both faster and smaller in magnitude compared to those of large animals.

Computer assisted lameness analysis with motion capture systems or inertial measurement units, IMUs, is becoming more and more common in horse clinics today as a more objective tool to evaluate and assess lameness. Data is collected during exercise and analyzed in a computer program after which movement asymmetries can be assessed. These methods can be helpful both in everyday activities and in more complicated cases, as the asymmetries can be monitored over time.

To our knowledge there is no similar commercial tool available for companion pets such as dogs yet. However, in a recent study at SLU which evaluated the use of IMUs on dogs trotting on a treadmill using a commercial system for horses with a modified software, good results were seen in moderate induced lameness scenarios. More studies are desirable to determine whether or not the method can be used in less controlled forms, e.g., in a hallway or in a corridor at a veterinary clinic.

The purpose of the this work has therefore been to investigate whether it is feasible to use standard IMUs, signal processing and software algorithms to reliably assess lameness of grade 2-3 in dogs under conditions prevailing at a regular veterinary clinic.

Thirteen clinically sound dogs were included in the study. None of the them had a history of orthopedic conditions or joint surgery. Reversible distal limb disturbances were induced, mimicking supporting limb lameness, in all dogs by placement of cotton wool wads under the paw. Reversible proximal limb disturbances, mimicking swinging limb lameness, were induced by placement of a custom-made weight above the carpus or tarsal joint, respectively. In order to obtain measurements we utilized a commercial measurement system developed by Delsys Inc. We used four IMUs in parallel located at the head, wither, pelvis and at one of the forelimbs. The data was analyzed offline using different algorithms for lameness assessment.

The results indicate that it possible to use standard IMUs to evaluate lameness in dogs, but that more work is needed to robustify the algorithms. Compared to horses the physical behavior of dogs and their smaller sizes leads to new challenges that need to be addressed in future research.

CONTENTS

1 INTRODUCTION

LAMENESS or other disturbances in the locomotor system (musculoskeletal system) are common reasons why dog owners seek veterinary care. The lameness is most often associated with pain or injury.

Evaluation of lameness have traditionally been performed subjectively by means of visual assessment and scoring. Such methods are well established in field of equine medicine where the examiner typically observes the vertical (ventro-dorsal) movements of the head and the pelvis during trotting locomotion. Unfortunately, the situation becomes more challenging when it comes to companion pets such as dogs, as their movements are both faster and smaller in magnitude compared to those of large animals.

Lameness analysis with motion capture systems or inertial measurement units (IMUs) is becoming more and more common in horse clinics today as a more objective tool to evaluate and assess lameness. Examples of commercially available systems are for instance the QHorse (motion capture) developed by QUALISYS AB, the Equinosis® Q with Lameness Locator® (IMU) developed by Equinosis Inc, and GaitSmart™ Pegasus (IMU) developed by ETB Ltd. Data is collected during exercise and analyzed in a computer program after which movement asymmetries can be assessed. These methods can be helpful both in everyday activities and in more complicated cases, as the asymmetries can be monitored over time.

There is no similar commercial tool available for dogs yet. However, in a recent study that tested IMUs on dogs trotting on a treadmill using the Lameness Locator® with a modified software (Rhodin et al., 2017), good results were seen in moderate induced lameness scenarios. More studies are desirable to determine whether the method can be used in less controlled forms, e.g., in a hallway or in a corridor at a veterinary clinic.

1.1 Purpose

The purpose of the study is to investigate whether standard inertial measurement units (IMUs) can be used to reliably assess lameness in dogs under conditions prevailing at a regular veterinary clinic. The work is part of a larger study involving also treatment options for dogs suffering from chronic pain. The feasibility of *transcutaneous electrical nerve stimulation* (TENS) will be evaluated in a blinded study.

2 LITERATURE REVIEW

Since the thesis work is a mixture between veterinary medicine and signal processing applications, the literature review will be divided into separate subsections. Section 2.1 gives a brief background to lameness, defines the basic concepts and describes how lameness can be assessed and graded. Section 2.2 gives a short introduction to inertial measurement units (IMUs). Section 2.3, finally, provides a survey regarding previous and related work using IMUs for lameness assessment.

2.1 Lameness

Lameness refers to an inability to properly use one or more limbs. It is most often associated with pain or injury. The most common causes of acute or sudden lameness in dogs are injury to a joint, muscle, bone fracture or dislocation. Osteoarthritis and hip dysplasia may also cause lameness in dogs. Lameness can affect dogs of any age from growing puppies to senior dogs.

2.1.1 Gait Analysis

The movement pattern of a four legged animal, e.g. a dog, can be described using *stride cycles*, where an entire cycle involves all four limbs taking a step forward. During each stride, every limb has a *stance phase* when it is in contact with the ground and a *swing phase* when it moves forward in preparation for the next stance phase. Loading of the limbs during the stance phase occurs in two stages. Immediately after the toes contact the ground the foot is rapidly decelerated giving rise to a shock wave that travels proximally through the bones and joints during the so-called *impact phase*. During the remainder of the stance phase, the limb is loaded more gradually as it accepts the body weight then pushes off against the ground. In general, the hard tissues (bones and joints) are more vulnerable to injury during the impact phase, whereas the soft tissues are more likely to be injured during the latter loading phase (Back and Clayton, 2013).

2.1.2 Lameness Assessment

Evaluation of the severity of the lameness has traditionally been performed subjectively by means of visual assessment. Such methods are well established in field of equine medicine where the examiner typically observes the vertical (ventro-dorsal) movements of the head and the pelvis during locomotion in order to identify the lame limb(s). The principle is that in a healthy non-lame animal the vertical displacements of these structures will have the same amplitude regardless of the limb bearing weight. A lame animal, though, will put more weight on the healthy limb than on the lame limb, so that the displacement becomes asymmetrical. Once the lame limb(s) is/are identified the degree of lameness is graded according to grading scale, for instance the one shown in Table 1.

Figure 1 (a) shows an artificial simulated example of the vertical (ventro-dorsal) displacement of the pelvis during trotting as function of time for an animal with a hindlimb lameness.

Table 1. *Lameness grading scale.*

Grade	Description
0	Normal, no lameness
1	Off weight bearing at a stance, no lameness noted at a walk/trot
2	Mild lameness at a trot, none at a walk
3	Moderate lameness at a walk/trot
4	Places foot when standing, intermittently carries limb when trotting
5	Non-weight bearing lameness

There are two max peaks and two min peaks (valleys) for each stride, since when one hindlimb is in stance phase the contralateral limb is in swing phase and vice versa. The amplitude of the displacement is larger for the healthy limb compared to the lame limb. The lowest position of the pelvis occurs in the middle of the loading phase, and the highest position occurs at the push off.

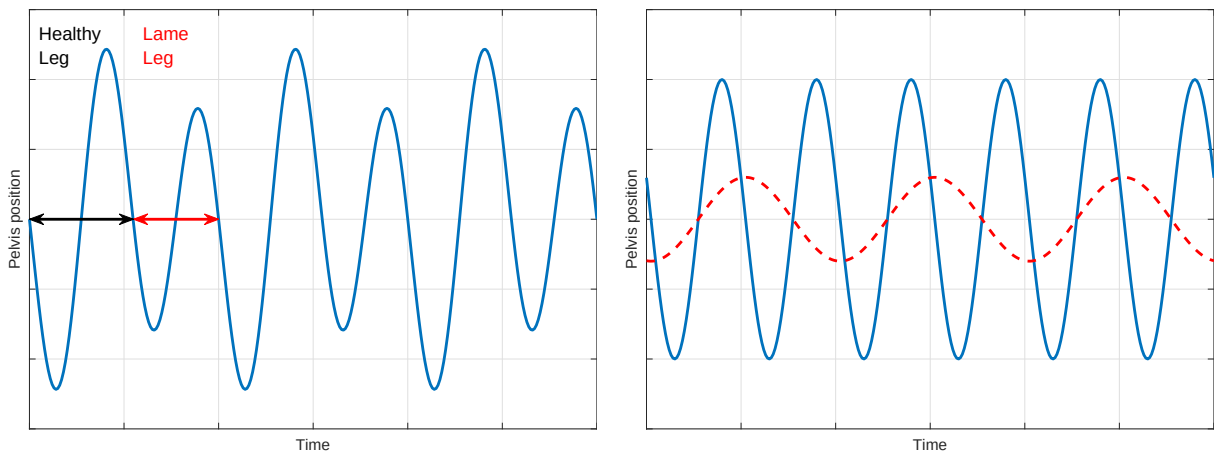

(a) (b)

Figure 1. *(a) A simulated example of hindlimb lameness. The animal will put more weight on the healthy limb than on the lame limb. (b) The lameness curve in (a) can be split up in two components; a non-lame component (blue/solid) and a lame component (red/dashed).*

It is straightforward to show that the (ideal) displacement curve in Figure 1 (a) can be split into a sum of two sinusoid components; a non-lame component with a frequency twice the stride frequency (shown as the blue/solid line in Figure 1 (b)) and a lame component with a frequency equal the stride frequency (shown as the red/dashed line in Figure 1 (b)).

The method for lameness assessment and grading described above can of course also be utilized for companion pets such as dogs. Unfortunately, the situation often becomes more challenging in this case, as the movement patterns of dogs are both faster and smaller in magnitude compared to those of large animals. The use of the head displacement as an indicator of forelimb lameness is also questionable. Dogs are more flexible in using their heads during exercise and often seek eye contact with their handlers. It is probably better to use the displacement of the withers as an indicator of forelimb lameness.

A general problem using the above described method is also that it is a *subjective method*, i.e., different examiners will probably arrive at different results. In a study done by Keegan et al. (2010) it was reported that when a group of clinicians (average 18.7 years of experience) were asked to choose whether or not a horse was lame and choose the worst limb, after full lameness evaluation, the clinicians agreed on the diagnosis only 51.6% of the time. Similar results have been reported for dogs. Waxman et al. (2008) measured ground reaction forces in dogs with induced supporting lameness, after visual scoring by three orthopedic surgeons and three veterinary students. The agreement between the visual assessment and the force plate data was low (0–39% agreement), depending on the degree of lameness. The authors concluded that subjective evaluation of lameness varied greatly between observers and that it agreed poorly with objective measures of limb function, such as ground reaction forces.

In order to get a more objective measure we will therefore investigate the use of inertial measurement units for lameness assessment.

2.2 Inertial Measurement Units (IMUs)

An inertial measurement unit, IMU, is a device that combines accelerometers and gyroscopes to produce a three dimensional measurement of both specific force and angular velocity with respect to an inertial reference frame. Sometimes the IMU is also complemented with magnetometers that sense the magnetic field around it and provide compass data (Wikipedia contributors, 2018). The number of independent sensors in the IMU defines the degrees of freedom (DOF). An IMU containing three accelerometers, three gyroscopes and three magnetometers is thus referred to as a 9-DOF IMU.

Traditionally IMUs have been expensive mechanical systems preserved military or aviation application use. However, with the advent of smart phones and hand-held video cameras etc, cheap on-chip IMUs have become widely available. These so-called MEMS (microelectromechanical systems) are equipped with miniature accelerometers that contain silicon beams, which deform during acceleration. Changes in capacitance are sensed within the chip, which outputs a voltage proportional the applied acceleration. Similarly, the MEMS contain miniature gyroscopes that sense Coriolis forces when rotations are applied to a pair of oscillating tines. Thus a voltage proportional to the applied rotational velocity is outputted. MEMS components are small, light, inexpensive, have low power consumption and short start-up times. However, they are still not performing as well as conventional high-grade sensors in view of misalignment, noise and temperature varying biases (offsets).

2.2.1 Accelerometers

The accelerometers are positioned orthogonally to each other, thus defining a local coordinate system. In this document we have adopted the right-hand NED (north-east-down) convention shown in Figure 2. That is, the x-axis points in the forward longitudinal (caudo-cranial) direction, the y-axis points in the right lateral direction, and the z-axis points in the vertical downward (dorso-ventral) direction. The numerical values obtained from the accelerometers

are given relative the gravity constant $g \approx 9.81\ m/s^2$, and we denote them a_x, a_y and a_z respectively. This means that if the IMU is in rest and perfectly aligned with the ground plane, then $a_x = a_y = 0$ and $a_z = -1$. In practice, though, the measured values are typically cor-

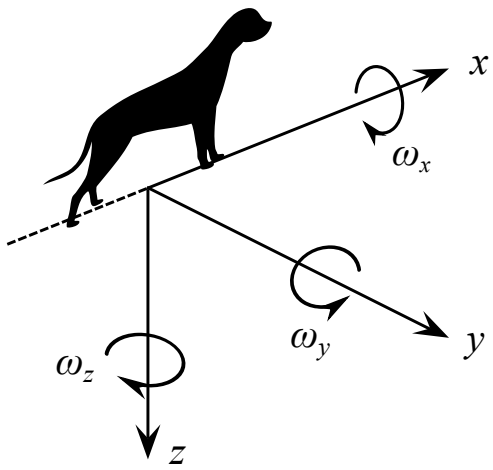

Figure 2. *The right-hand north-east-down (NED) coordinate system.*

rupted by biases and measurement noise. We assume that they consist of the true specific force a^0, a slowly varying bias term b^a, and measurement noise e. That is,

$$a_i = a_i^0 + b_i^a + e_i, \qquad i \in \{x,\ y,\ x\}. \tag{1}$$

2.2.2 Gyroscopes

The gyroscopes are oriented so that they measure the rotational velocities around the x-, y- and z-axes as shown in Figure 2. Their positive directions are clockwise while looking along the axes. We denote the measured values ω_x, ω_y and ω_z. They are commonly referred to as the *roll* angle velocity, the *pitch* angle velocity, and the *yaw* angle velocity, respectively. As for the accelerometers above, we assume that the measured values consist of the true angle velocity ω^0, a slowly varying bias term b^g, and measurement noise v. That is,

$$\omega_i = \omega_i^0 + b_i^g + v_i, \qquad i \in \{x,\ y,\ x\}. \tag{2}$$

2.2.3 Using Inertial Data in Applications

When using the data from inertial sensors, one is often interested in obtaining the position in the 3D (x-y-z) space and the rotation angles around the axes (orientation or attitude). In order to do so the signals from the IMU have to be integrated; the angular velocities once to obtain the angles, the accelerations twice to obtain the displacements. A major drawback with MEMS components in this regard is that the noise and biases in the measurements will contribute to severe drifts in the integrated signals. Thus some form of filtering (e.g., low-pass filtering to get rid of noise, and high-pass filtering to get rid of biases and trends) and/or sensor fusion is required. Another complication is that the measurements are given relative the local coordinate systems of the IMUs, i.e., the *IMU frames*. Sometimes one is instead interested in

the positions and orientations of the IMUs relative the earth coordinate system, i.e., the *earth frame*. A system that estimates those quantities is called an *attitude and heading reference system* (AHRS). Different approaches for AHRSs have been thoroughly studied within the fields of avionics and robotics. I have in this work investigated the use of an Extended Kalman filter (EKF) based on quaternions, see Appendix B. Knowing the attitude might be advantageous when selecting valid trotting data, and for correction of the accelerometer signals.

2.3 Lameness Assessment Using IMUs

Lameness assessment using IMUs is not a new idea. A significant amount of work has been carried out within the field of equine medicine, see for instance Keegan et al. (2004), Pfau et al. (2005), Pfau et al. (2013) and the references therein. There also exist commercial IMU-based tools for horses. Equinosis® Q with Lameness Locator® (formerly known as just Lameness Locator®), is based on the work by Keegan et al. (2011). This system utilizes three IMUs; one on the head, one on the left forelimb, and one on top of the pelvis. Another commercial system is GaitSmart™ Pegasus which uses IMUs within brushing boots and a GPS sensor on the rider's hat. A third system under development is EquiMoves (Bosch et al., 2018) which works by capturing horse motion from up to eight synchronized wireless IMUs. In their work they did put IMUs on all four limbs which enables them to also evaluate the limb angles for the individual limbs.

A quite recent study performed by Rhodin et al. (2017) at SLU investigated the performance of IMUs on dogs trotting on a treadmill using the Lameness Locator® with a modified software. They obtained good results for moderate induced lameness scenarios. Jenkins et al. (2018) have developed and validated an IMU method for automatic canine gait analysis using a single wearable sensor put on the animals leg during exercise on a treadmill. Ladha et al. (2017) have developed *GaitKeeper*, a system for measuring and analyzing canine gait using four IMU sensors; one on each leg.

3 MATERIAL AND METHODS

The aim of the study is to investigate whether standard IMUs can be used to reliably assess lameness in dogs under conditions prevailing at a regular veterinary clinic. The Ethical Committee for Animal Experiments, Uppsala, Sweden (No. C67/16) approved the study, which was performed with the informed consent of the dog owners.

3.1 Animals

Thirteen clinically sound dogs were included in the study (six Labrador Retrievers, two Riesen Schnauzers, two mixed breed dogs, one Lagotto Romagnolo, one Nova Scotia Duck Tolling Retriever, and one Pointer). They were all belonging to staff or students at SLU who had shown interest in participating in the study in response to a small email and social media campaign at the campus. There were five males and eight females. Mean age was 5.1 $\pm$ 3.3 years, and mean height at the withers was 53.6 $\pm$ 6.0 cm. The dogs were assessed as clinically sound after orthopedic examination performed by the supervisor Dr Anna Bergh. None of the dogs had a history of orthopedic conditions or joint surgery.

3.2 Lameness Induction

Reversible distal limb disturbances were induced, mimicking supporting limb lameness, in all dogs by placement of a cotton wool wad under the paw, secured with cohesive bandage. The size of the wad was adjusted to each dog to induce lameness of 2-3 degrees (on a scale 0–5 according to Table 1: moderately lame, distinctly visible at the trot). Proximal limb disturbances, mimicking swinging limb lameness, were reversibly induced by placement of a custom-made weight (200 g) above the carpus or tarsal joint, respectively. Assessment and grading of the resulting lameness induction was performed by the supervisors Dr Anna Bergh and Anja Pedersen.

3.3 Instrumentation

In order to obtain IMU data we have used a commercial measurement system, Trigno™ Wireless EMG[1], developed by Delsys Inc. The system provides the possibility to use up to sixteen IMUs in parallel. The measured data were sampled with a frequency of $f_s = 148.15$ Hz and transmitted wirelessly over a custom RF protocol operating within the 2.4 GHz spectrum to a base station connected to a computer via USB. The measurements were recorded to files using the software that was provided by the system, *EMGWorks Acquisition*. Each IMU (called Trigno™ Avanti) is a small 9-DOF unit complemented with an electromyography (EMG) sensor that can measure the electrical activity produced by skeletal muscles, see Figure 3 (a). Each unit measure 37 $\times$ 26 $\times$ 15 mm and weigh approximately 14 grams. The four metal bars at the bottom of the unit are normally attached to the skin and measure the muscle activity under the

[1] https://www.delsys.com/products/wireless-emg/

(a) (b)

Figure 3. *(a) The Trigno™ Avanti IMU used for data collection. (b) The base station. Images: © Delsys Inc.*

sensor. However, these measurements have not been utilized in this work. Figure 3 (b) shows the base station.

In our trials we used four IMUs located according to Figure 4. The IMUs were attached to

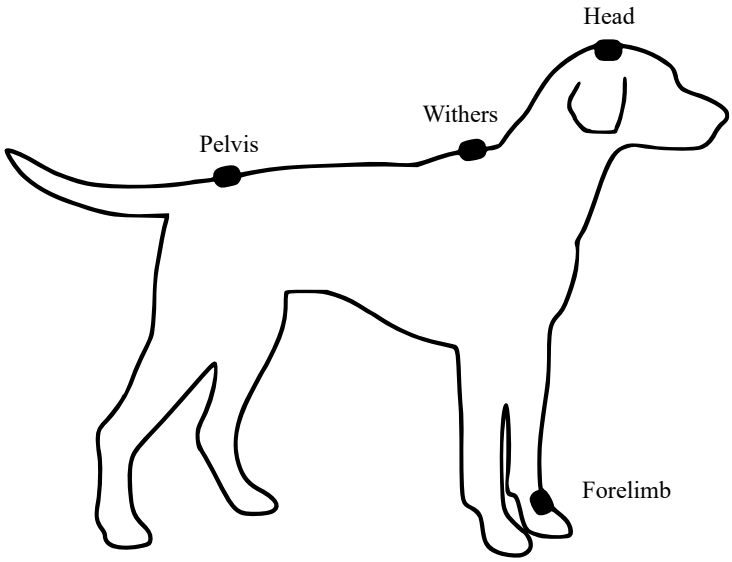

Figure 4. *Sensor placement during the trials.*

the animals using a combination of home-made textile harnesses, Velcro and double adhesive tape, see Figure 5. The IMUs on the head, withers and pelvis were oriented so that their x-axes were pointing cranially in the median plane. The IMU on the forelimb was oriented with its x-axis pointing proximally along the leg. A dummy sensor was attached to the contralateral forelimb in order to not induce lameness by the instrumentation. The coordinate system convention for the Trigno™ Avanti IMU seems be WSU (west-south-up). However, since we were not using the EMG sensor we decided to put Velcro on top of the IMUs and flipped them upside down, hence arriving at an ESD (east-south-down) orientation. Thus, in order to obey the NED convention shown in Figure 2, the IMU coordinate system had to be rotated $-90°$ around

(a) (b)

Figure 5. *Examples of sensor attachments.*

the z-axis. That is, to flip the x and y measurements and negate the measurements associated with the x-axis.

3.4 Measurement Procedure

In addition to the IMUs we also used a pressure mat system, Tekscan Walkway™ High Resolution[2], to record data. Briefly, pressure mat analysis is a system in which the weight-bearing forces can be estimated as the animal steps onto a sensor mat during locomotion (DeCamp et al., 2016). Analysis of pressure mat data is performed in another project and will not be considered further in this work.

Data were collected while the dogs were trotting back and forth in a corridor with 180° turns in the end, stepping on the pressure mat in each direction. A handler was running with the dogs to ensure that they kept the right path and right steady-state trotting pace. The handler controlled the dogs via a leash.

One measurement session was performed before the first lameness induction (sound trial) and then during each lameness induction in one limb at a time. The lameness inductions described in Section 3.2 were induced in one forelimb and one hindlimb, yielding four trials of induced lameness per dog. Extra sound trials were collected between the induced measurements to ensure return to soundness. In total, data from eight registration sessions were collected for

[2] https://www.tekscan.com/product-group/medical/mats-and-walkways

each dog, and a recovery period was allowed between the trials since all data had to be processed and saved to file.

3.5 Data Analysis

After successful data collection, the data were exported to CSV files and imported into the data analysis tool MATLAB (MathWorks, 2018). Nine signals,

$$a_x,\ a_y,\ a_z,\ \omega_x,\ \omega_y,\ \omega_z,\ m_x,\ m_y,\ m_z, \tag{3}$$

sampled with sampling period $T_s = 1/f_s = 6.7$ ms were obtained for each IMU where a, ω and m denote acceleration, angular velocity, and magnetometer data respectively. In the sequel we use superscript h (head), w (withers), p (pelvis) and f (forelimb) to indicate the sensor in question, so that for instance a_z^p means the vertical acceleration measurement from the pelvis sensor. We also use square brackets to denote sample index, that is,

$$a_z[k] = a_z(kT_s), \tag{4}$$

denotes the sampled version of the continuous signal $a_z(t)$ at sample instant k.

The data for each trial (consisting of in total $4 \times 9 = 36$ signals) was aligned to a common time frame and was saved to a separate MATLAB "mat-file" along with meta data regarding the trial, such as *dog name*, *breed*, *lameness grade* etc. The lameness grade was specified per limb, so that each trial contains four grade values, Grade_{FL}, Grade_{FR}, Grade_{HL} and Grade_{HR}, associated with the fore left, fore right, hind left and hind right limbs respectively.

3.5.1 Attitude and Heading Estimation

The data was first transformed from the IMU reference frames to the earth reference frame using the quaternion-based AHRS algorithm outlined in Appendix B. An AHRS (attitude and heading reference system) algorithm fuses the information from several sensor sources in order to enhance the attitude estimation. With attitude here we mean the orientation in the earth frame expressed in *Euler angles* ϕ (roll), θ (pitch) and ψ (yaw), see Section B.2.1 in Appendix B.

The accelerometer and gyroscope data, $a[k]$ and $\omega[k]$, from the three IMUs located on the pelvis, withers and head were included in the extended Kalman filter (EKF) described in Section B.3. We decided to only include the gyro offsets in the filter (that is, treating the accelerometer offsets as noise) yielding a final filter consisting of 21 states (3×4 quaternion components + 3×3 gyro offsets). The filter states of each IMU were initially assumed to be independent of those of the other IMUs, so that the 21-state filter is equal to running three 7-state filters in parallel. Since the interesting bandwidth of the attitude dynamics is well below 10 Hz, the data was resampled from 148.15 Hz to 20 Hz before the EKF was applied.

The fact that several dogs were shaking intermittently during the trials (probably because of the instrumentation) had a bad impact on the stability of the EKF. This was remedied by calculating a sliding window variance of the angular velocity $\omega_x[k]$ around the caudo-cranial x-axis, and by blocking the measurement update in the filter when this variance was high.

A problem with using only gyroscope and accelerometer data (i.e., a 6-DOF IMU) is that the accelerometers will not be able to stabilize the yaw (heading) estimate. A common solution is thus to utilize the magnetometer (compass) measurements $m[k]$ in order to stabilize the yaw. Here we decided not to use the magnetometer data since we were performing the experiments indoors were the magnetometers are prone to magnetic disturbances (electronic equipments, iron in the building etc).

Figure 6 (a) shows the result when estimating the Euler angles for the pelvis IMU in one example trial. From the figure we can see that the filter is not able to stabilize the yaw, so that

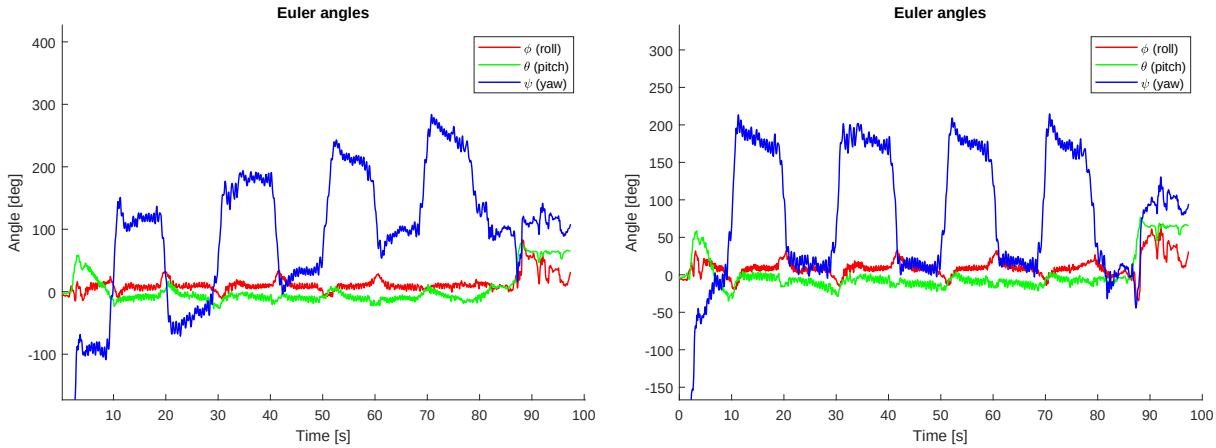

(a) (b)

Figure 6. *Euler angles estimated using the extended Kalman filter. (a) Without yaw constraint. (b) With yaw constraint.*

we get a drift in the estimate. The 180° turns in the ends of the corridor are clearly visible though. A drift in the yaw estimate is not a big deal if the goal is to just compensate the accelerometer signals. However, if we would like to use the yaw for data segmentation, it could be advantageous with a drift-free estimate.

A possible option to stabilize the yaw estimates is to add a constraint to the filter requiring that the angles must be a multiple of 180° (see Appendix B). Running the filter with this constraint gives the result shown in Figure 6 (b). Another option is to introduce dependencies between the states of the three IMUs. This can be achieved by augmenting the Kalman filter with virtual measurements that aims at keeping the yaw estimates approximately equal. A third option to stabilize the yaw is to utilize GPS sensors, but the indoor experimental setup will likely reduce the usefulness of such devices.

3.5.2 Segmentation

The data was then split in segments containing valid trotting data by applying a Pearson sliding window correlation operation to the vertical accelerometer signals from the withers and pelvis sensors, a_z^w and a_z^p, and thresholding the result. That is,

$$r_k = \frac{\sum_{i=k-P+1}^{k} \left(a_z^w[i] - \bar{a}_z^w\right)\left(a_z^p[i] - \bar{a}_z^p\right)}{\sqrt{\sum_{i=k-P+1}^{k} \left(a_z^w[i] - \bar{a}_z^w\right)^2}\sqrt{\sum_{i=k-P+1}^{k} \left(a_z^p[i] - \bar{a}_z^p\right)^2}}, \tag{5a}$$

where

$$\bar{a}_z^w = \frac{1}{P} \sum_{i=k-P+1}^{k} a_z^w[i], \tag{5b}$$

$$\bar{a}_z^p = \frac{1}{P} \sum_{i=k-P+1}^{k} a_z^p[i], \tag{5c}$$

denote the sample means and P is the window width. Figure 7 shows an example of the result of segmentation. A value of 1 in the binary/red curve indicates that the data will be used for stride analysis. The pelvis vertical acceleration a_z^p is also shown for reference.

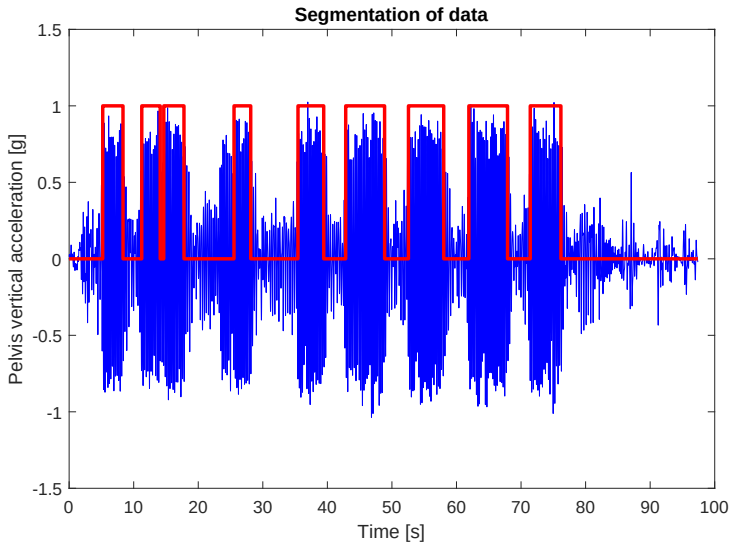

Figure 7. *Data segmentation. A value of 1 in the binary signal (red) indicates that data represent trotting and thus will be included in the analysis.*

3.5.3 Stride Splitting

Stride splitting (i.e., extracting data associated with individual strides) within the valid trotting segments was achieved by using data from the IMU at the forelimb to identify left or right stance or swing phase. The accelerometer signal along the cranio-caudal z-axis, a_z^f, was zero-phase filtered with 4th order Butterworth high-pass filter with cutoff frequency 0.5 Hz and double integrated using the trapezoidal rule (see Appendix A) in order to obtain the displacement p_z^f as shown in the example in Figure 8 (a). The time instants for "toe on", i.e., when the toes touches the ground in the beginning of each stance, were determined by identifying the min peaks which are indicated as dashed lines in the plot. The min peaks represent the most cranial position of the limb, and occurs just before the toes hit the ground. Figure 8 (b) shows the corresponding acceleration along the caudo-cranial z-axis, a_z^f. This is in accordance with the similar result for horses reported by Olsen et al. (2012) and Bragança et al. (2017).

The vertical displacements for the withers p_z^w and pelvis p_z^p were then computed similarly to the frontlimb position above, by double integrating the accelerometer signals a_z^w and a_z^p.

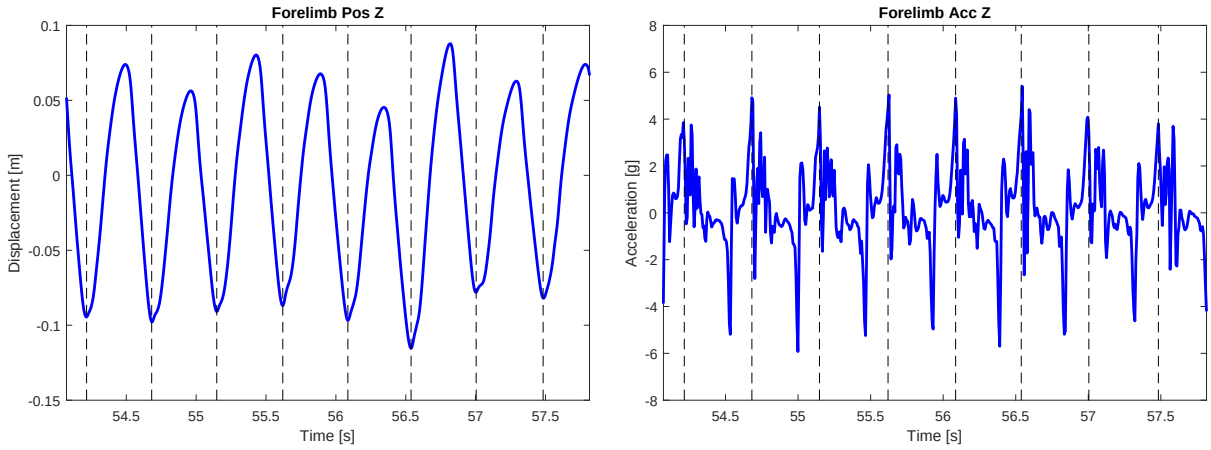

(a) (b)

Figure 8. *Stride splitting using the forelimb IMU. The dashed lines represent the most cranial positions of the frontlimb, which occur just before "toe on".*

Here we decided to do the integration in the frequency domain instead (see Appendix A) since that resulted in a slightly better result. While in the frequency domain, the signals were band-pass filtered in the frequency range between 1 to 6 Hz before the signals were transformed back to the time domain. The frequency range was selected after analyzing all trials, in which the average stride frequency while trotting was around 2 Hz.

The displacement signals were then split according to the "toe on" time instants described above to in order to obtain withers and pelvis data associated with the strides, see Figure 9. One problem, however, with the data on this form is that the length of the time intervals defined

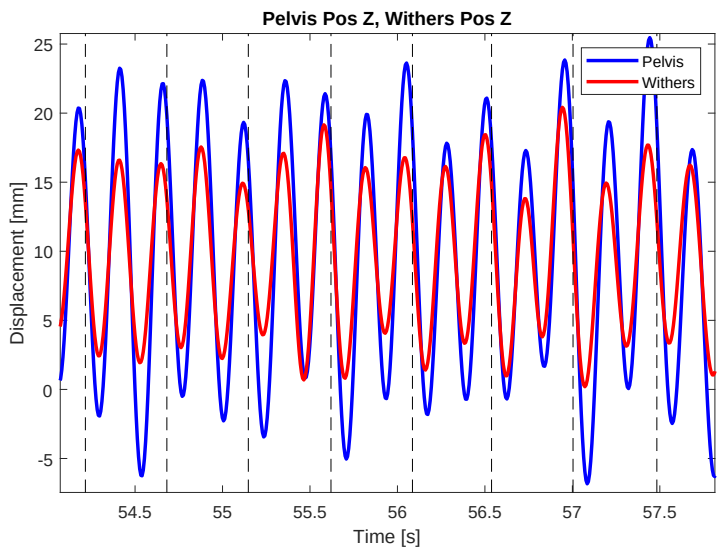

Figure 9. *Stride split of withers and pelvis vertical positions p_z^w and p_z^p.*

by "toe on" in general are different as they depend on the trotting speed. As a last step in the preprocessing of data, the time instants for the stride data were therefore normalized to the unit

interval [0, 1] and interpolated/resampled to a common time frame of M samples, i.e.,

$$\tau_k = \frac{k-1}{M}, \qquad k = 1, \ldots, M. \tag{6}$$

Figure 10 shows examples of time normalized strides from the pelvis sensor in two different trials; a sound trial in Figure 10 (a), and a trial with induced swinging hindlimb lameness in Figure 10 (b). By smoothing the plots (averaging) with the eye it is rather clear that the curves

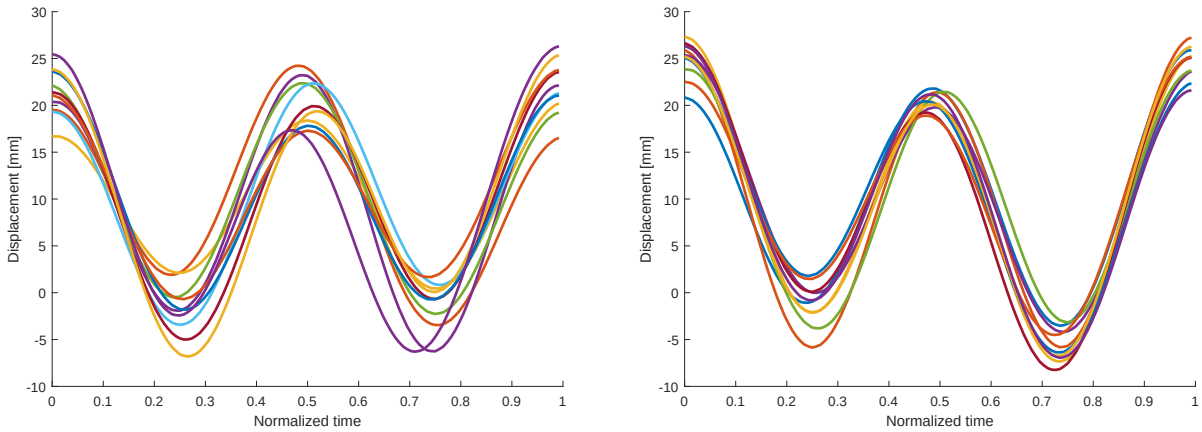

(a) (b)

Figure 10. *Time normalized pelvis strides p_z^p from two different trials. (a) Sound trial. (b) Trial with hindlimb swinging lameness.*

are consistent with the trial setup. An induction on a hindlimb was always done on the limb diagonal to the forelimb carrying the sensor. Thus the lame stance will occur first which is evident from Figure 10 (b).

I also compared the above described filtering and integration procedure with the cyclic integration method proposed by Pfau et al. (2005), but did not get any improvements while using their method.

3.5.4 Min and Max Peak Statistics

One obvious path to explore is to analyze the min and max peak statistics for the withers and pelvis displacements in the vertical (dorso-ventral) direction. This is the same method as has been considered in the Lameness Locator® and similar systems. Let us return to the simulated example we used earlier in Section 2.1.2. Figure 11 shows the min and max peaks in the pelvis displacement p_z^p for an animal with hindlimb lameness. The idea is to form the quantities $\mathrm{PD}_{\min}$ and $\mathrm{PD}_{\max}$, which denote the differences in min peaks and max peaks amplitudes for the pelvis respectively, i.e.,

$$\mathrm{PD}_{\max} = \mathrm{Max}_1 - \mathrm{Max}_2, \tag{7a}$$

$$\mathrm{PD}_{\min} = \mathrm{Min}_2 - \mathrm{Min}_1, \tag{7b}$$

and analyze them statistically. Analogously we form the quantities $\mathrm{WD}_{\min}$, $\mathrm{WD}_{\max}$, $\mathrm{HD}_{\min}$ and $\mathrm{HD}_{\max}$ for the withers and the head.

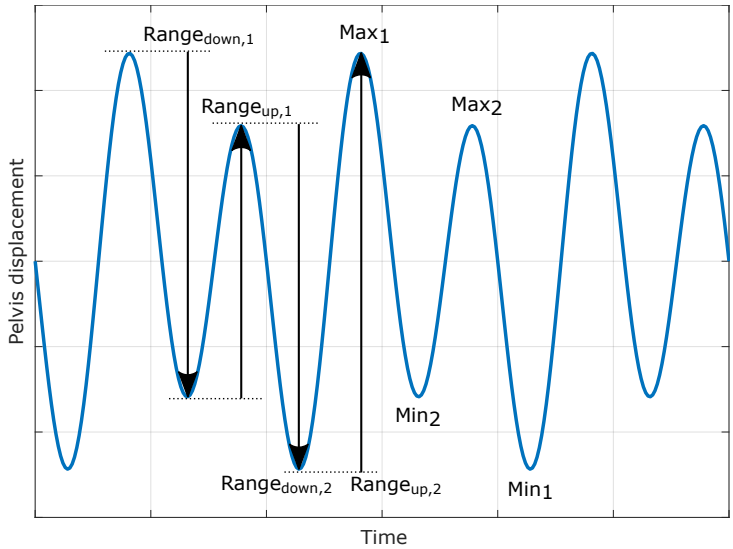

Figure 11. *Min and max peaks for the pelvis displacement* p_z^p.

Inspired by the work by Starke et al. (2012) and Bosch et al. (2018) the following quantities were also analyzed statistically (see Figure 11):

- $\text{Range}_{\text{down},1}$ and $\text{Range}_{\text{down},2}$: The difference in amplitude between the max peak and the min peak for the displacement in downward direction during a stance phase. Since there are two stance phases during each stride there will be two values.
- $\text{Range}_{\text{up},1}$ and $\text{Range}_{\text{up},2}$: The difference in amplitude between the min peak and the max peak for the displacement in upward direction during a stance phase. Since there are two stance phases during each stride there will be two values.
- $\Delta\,\text{Range}_{\text{down}}$: The difference between the two downward ranges.
- $\Delta\,\text{Range}_{\text{up}}$: The difference between the two upward ranges.

Then the upwards and downwards *symmetry indices* (SI) can be formed according to

$$\text{SI}_{\text{down}} = \frac{\Delta\,\text{Range}_{\text{down}}}{\max\left(\text{Range}_{\text{down},1}, \text{Range}_{\text{down},2}\right)} \tag{8a}$$

$$\text{SI}_{\text{up}} = \frac{\Delta\,\text{Range}_{\text{up}}}{\max\left(\text{Range}_{\text{up},1}, \text{Range}_{\text{up},2}\right)} \tag{8b}$$

An SI value of 0 indicates perfect symmetry, whereas a value of ± 1 indicates maximum asymmetry where the sign depends on the affected limb.

3.5.5 Fourier Series Analysis

Inspired by the work of Kasebzadeh and Gustafsson (2018), who have analyzed human gait using IMUs, I did also chose to investigate if frequency analysis could be utilized. The motivation behind this study was to see if it possible to avoid the steps of identifying the max and min peaks as are required in the method described in Section 3.5.4.

It is well known that every function $f(t)$ that is periodic on an interval $[t_0,\ t_0 + P]$ can be approximated by a sum of sine and cosine functions with increasing frequencies, see for instance Bracewell (1999). That is,

$$f_N(t) = \frac{\alpha_0}{2} + \sum_{k=1}^{N} \left(\alpha_k \cos \frac{2\pi k t}{P} + \beta_k \sin \frac{2\pi k t}{P} \right), \tag{9}$$

where

$$\alpha_k = \frac{2}{P} \int_{t_0}^{t_0+P} f(t) \cos \frac{2\pi k t}{P}\, dt, \tag{10a}$$

$$\beta_k = \frac{2}{P} \int_{t_0}^{t_0+P} f(t) \sin \frac{2\pi k t}{P}\, dt. \tag{10b}$$

The approximation $f_N(t)$ improves as $N \to \infty$ and the limit value $f_\infty(t)$ is called the *Fourier series* representation of $f(t)$ (Bracewell, 1999).

Fourier series techniques can be applied to the data representing the withers and pelvis displacements in the vertical (dorso-ventral) direction p_z using inspiration from equation (9) above and elementary matrix algebra. Let

$$\bar{p}_z = (p_z(\tau_1),\ p_z(\tau_2),\ \ldots,\ p_z(\tau_M))^T, \tag{11}$$

be a vector containing the M displacement data samples interpolated on the interval $[0,\ 1]$, and define

$$H_N = \begin{pmatrix} 1 & \cos 2\pi\tau_1 & \cdots & \cos 2\pi\tau_1 N & \sin 2\pi\tau_1 & \cdots & \sin 2\pi\tau_1 N \\ 1 & \cos 2\pi\tau_2 & \cdots & \cos 2\pi\tau_2 N & \sin 2\pi\tau_2 & \cdots & \sin 2\pi\tau_2 N \\ \vdots & \vdots & \vdots & \vdots & \vdots & \ddots & \vdots \\ 1 & \cos 2\pi\tau_M & \cdots & \cos 2\pi\tau_M N & \sin 2\pi\tau_M & \cdots & \sin 2\pi\tau_M N \end{pmatrix} \tag{12a}$$

$$\vartheta_N = (\alpha_0,\ \alpha_1,\ \ldots, \alpha_N, b_1,\ \ldots, b_N)^T. \tag{12b}$$

Then we can use the linear model

$$\bar{p}_z = H_N \vartheta_N, \tag{13}$$

and estimate ϑ_N using ordinary least squares, e.g.,

$$\hat{\vartheta}_N = \left(H_N^T H_N\right)^{-1} H_N^T \bar{p}_z, \tag{14}$$

where $(\cdot)^{-1}$ denotes matrix inverse and $(\cdot)^T$ denotes matrix transpose. If we just consider the stride and the double stride frequencies, then $N = 2$. The amplitudes of the lame and non-lame sinusoid components can thus be estimated using the expressions

$$\hat{A}_1 = \sqrt{\hat{\alpha}_1^2 + \hat{\beta}_1^2}, \tag{15a}$$

$$\hat{A}_2 = \sqrt{\hat{\alpha}_2^2 + \hat{\beta}_2^2}. \tag{15b}$$

so that the ratio

$$\varrho = \frac{\hat{A}_1}{\hat{A}_2} \tag{16}$$

can be used as a measure of lameness. Figure 12 shows an example of the result obtained after fitting a Fourier series model to the vertical displacement data in a stride.

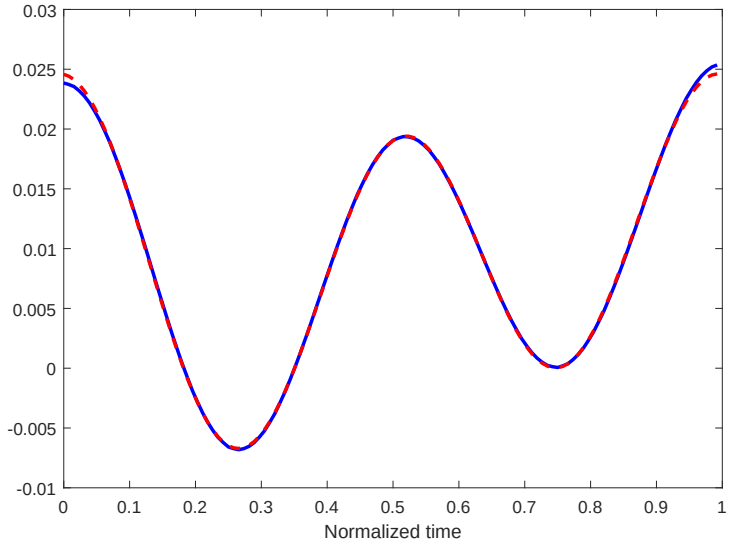

Figure 12. *Result after fitting a Fourier series model to the vertical displacement data in a stride (blue/solid: data, red/dashed: fitted model).*

4 RESULTS

Experimental data has been analyzed for 98 trials. The original plan was to record eight trials per dog, resulting in a total of $13 \times 8 = 104$ trials. Unfortunately though six trials have been discarded due to bad or absent data. There are in average 8.77 ± 3.31 segments of trotting data per trial. Counting the strides within these segments yields 86.4 ± 40.1 strides per trial. Bad strides, i.e., strides that do not show the shape according to Figure 12, have been discarded.

During the analysis the 98 trials have been classified as follows according to the lameness scale described in Table 1;

- **Sound**: Trials with $\text{Grade}_{\text{FL}} \leq 1$, $\text{Grade}_{\text{FR}} \leq 1$, $\text{Grade}_{\text{HL}} \leq 1$ and $\text{Grade}_{\text{HR}} \leq 1$,
- **Fore lameness**: Trials with $\text{Grade}_{\text{FL}} > 1$ or $\text{Grade}_{\text{FR}} > 1$, and $\text{Grade}_{\text{HL}} \leq 1$, $\text{Grade}_{\text{HR}} \leq 1$,
- **Hind lameness**: Trials with $\text{Grade}_{\text{HL}} > 1$ or $\text{Grade}_{\text{HR}} > 1$, and $\text{Grade}_{\text{FL}} \leq 1$, $\text{Grade}_{\text{FR}} \leq 1$.

We thus obtain 54 sound trials, 19 forelimb lameness trials, and 25 hindlimb lameness trials.

4.1 Min and Max Statistics

We start by analyzing the results of the min and max statistics described in Section 3.5.4. Figure 13 shows the box plots of the quantities WD_{min} and WD_{max} when evaluated on all trials. Here

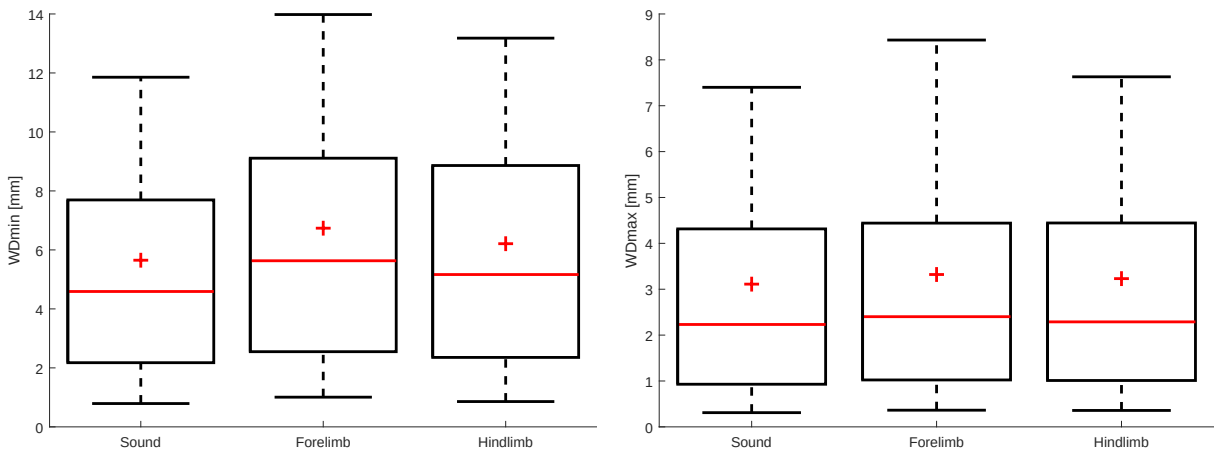

(a) (b)

Figure 13. *(a) Box plots of the min peak differences for the withers, WD_{min}. (b) Box plots of the max peak differences for the withers, WD_{max}.*

the red "+" symbol in the boxes denotes the mean value, and the horizontal red line in the boxes represents the median. The edges of the boxes are the 25th and 75th percentiles. The dashed vertical lines indicate variability outside the upper and lower quartiles where their ends represent the 9th and 91th percentile respectively. The first thing to note is that we seem to have

asymmetries present already during the sound trials. Furthermore we see that the results are correlated with the inductions, but the differences between sound and induced lameness trials are not as significant as we would wish.

Figure 14 shows analogously the box plots of the quantities PD_{min} and PD_{max} when evaluated on all trials. Here the results are more consistent with the lameness inductions, but we still have

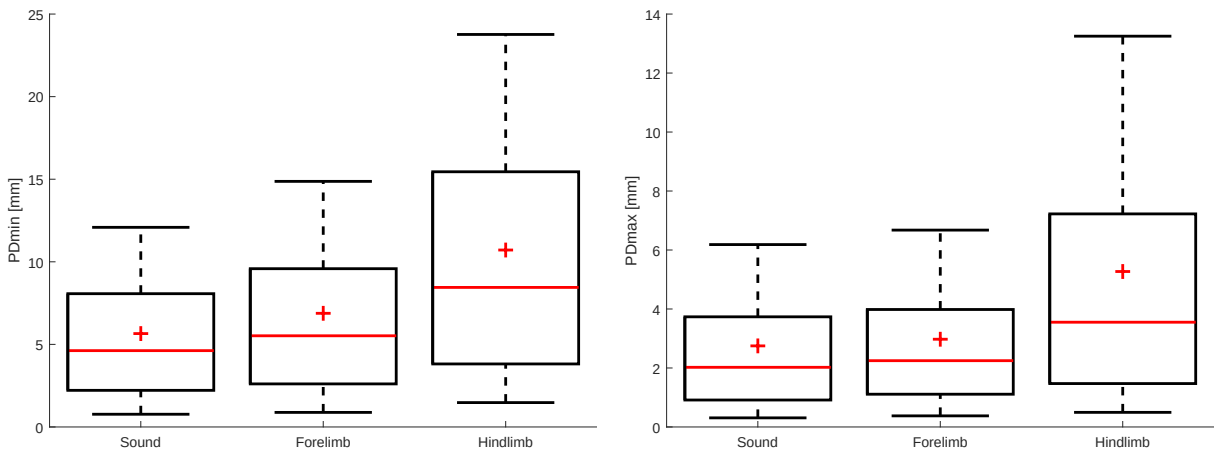

(a) (b)

Figure 14. *(a) Box plots of the min peak differences for the pelvis, PD_{min}. (b) Box plots of the max peak differences for the pelvis, PD_{max}.*

asymmetries present in the sound trials.

Figure 15 and Figure 16 show the corresponding statistics for the symmetry indices (SI_{down} and SI_{up}) defined according to equation (8) for the withers and the pelvis. Also here we see

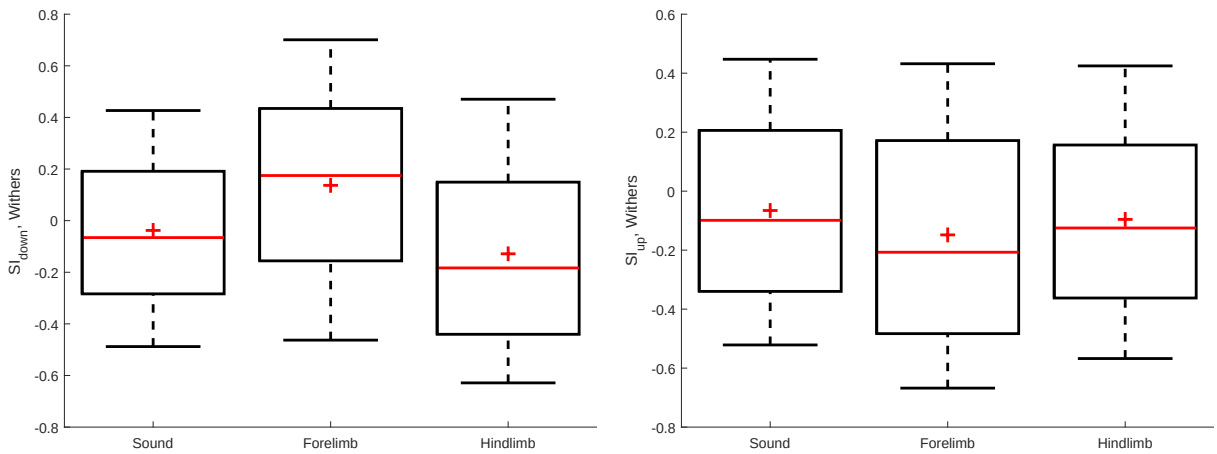

(a) (b)

Figure 15. *(a) Box plots of the symmetry index for the withers in the downward direction, SI_{down}. (b) Box plots of the symmetry index for the withers in the upward direction, SI_{up}*

that the symmetry indices are more correlated with the inductions at the rear limbs compared to those at the fore limbs. According to the definition in (8), the symmetry indices for the withers and the pelvis should have opposite signs since lameness was always induced on the diagonal

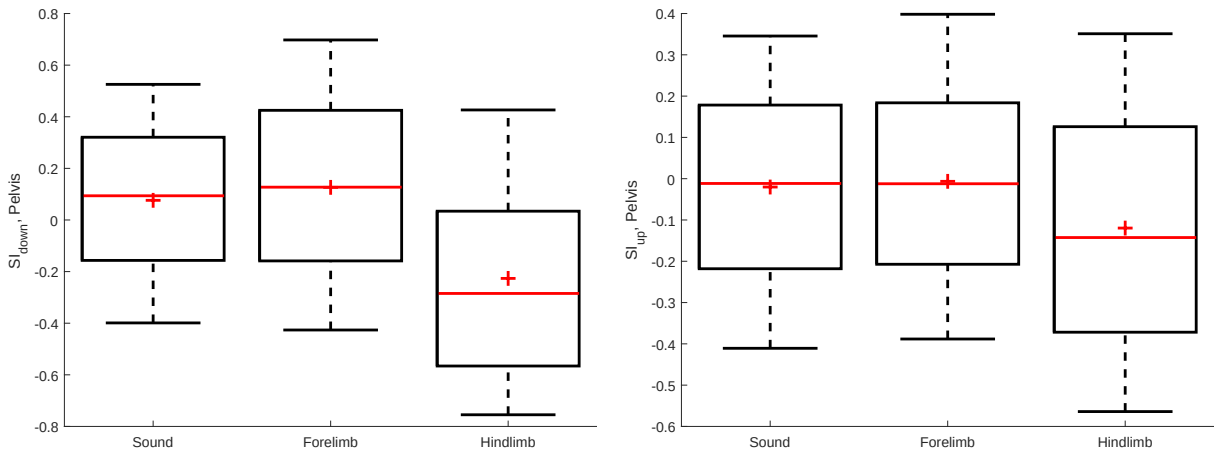

(a) (b)

Figure 16. *(a) Box plots of the symmetry index for the pelvis in the downward direction, SI_{down}. (b) Box plots of the symmetry index for the pelvis in the upward direction, SI_{up}.*

or contralateral limb relative the frontlimb carrying the sensor. At least the result in Figure 15 (a) and Figures 16 (a)-(b) are consistent with this fact.

If we analyze the max and min peak statistics while taking the induction type into account, we get the results shown in Figure 17 and Figure 18. Here `F-swing` denotes frontlimb swinging

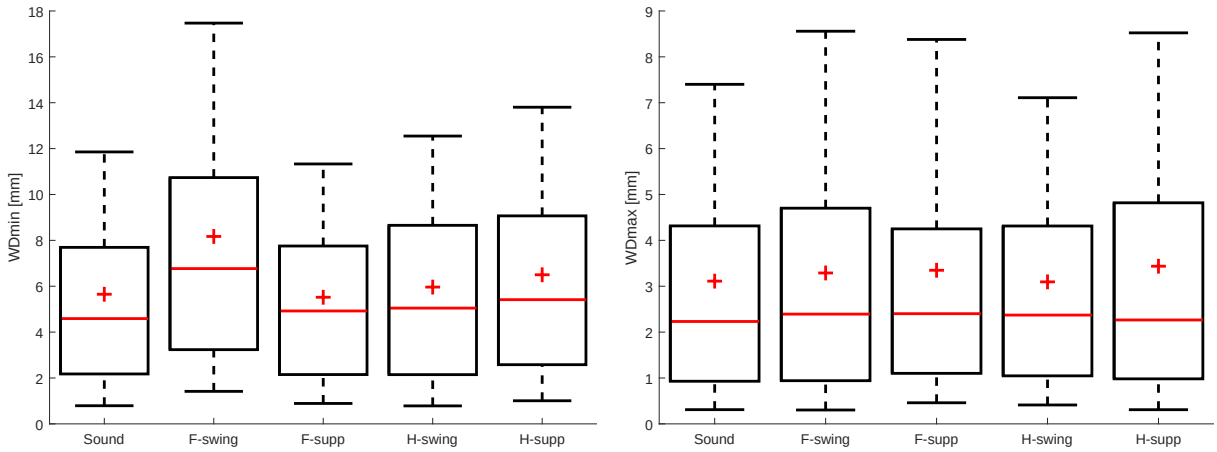

(a) (b)

Figure 17. *(a) Box plots of the min peak differences for the withers (WD_{min}) separated by induction type. (b) Box plots of the max peak differences for the withers (WD_{max}) separated by induction type.*

lameness, `H-supp` hindlimb supporting lameness etc. Also here it is evident that the algorithm performs better for the rearlimbs, with the exception of the max peak statistics for swinging lameness. For the forelimbs the algorithm seems to perform best for swinging lameness. The differences in performance for the front and rear limbs could be related to the fact that a dog, in contrast to a horse, in general has a much more loose and flexible skin, especially in the withers region. Thus the sensor at the wither will move more during locomotion and induce disturbances.

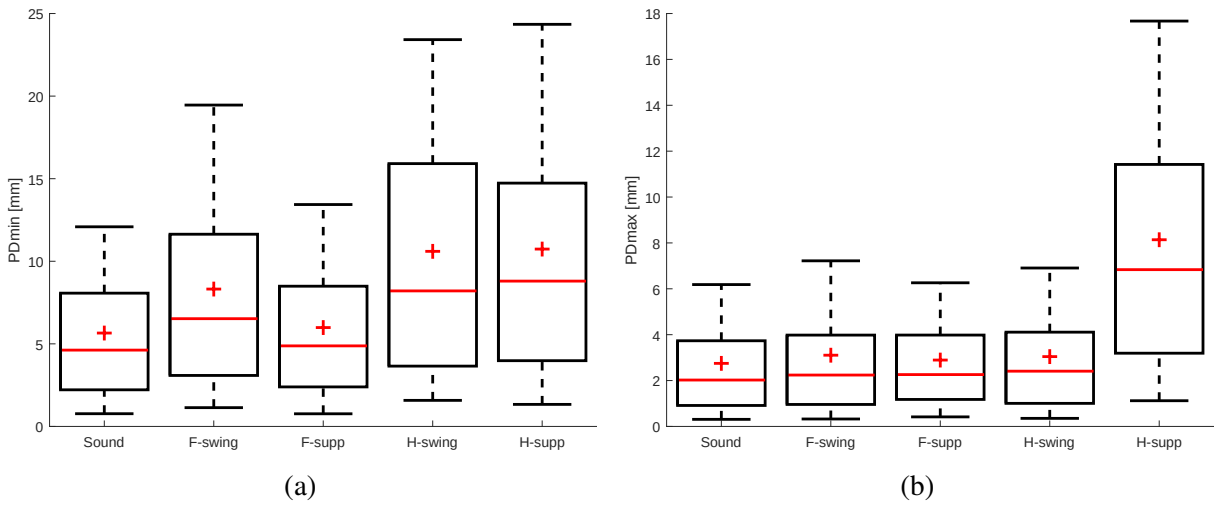

Figure 18. *(a) Box plots of the min peak differences for the pelvis (PD_{min}) separated by induction type. (b) Box plots of the max peak differences for the pelvis (PD_{max}) separated by induction type.*

It is worth to point out that the analysis has been carried out using all 98 trials. We will probably obtain better results if we exclude trials with inconsistent inductions. Exclusion can be done by analyzing the video films that were recorded during the trial sessions.

4.2 Frequency Analysis

It would also be of interest to analyze the performance of the frequency analysis approach outlined in Section 3.5.5. Figure 19 shows the statistics for the amplitude ratio ϱ defined in Equation (16). Here we see that the results are more consistent with the induction type. We can

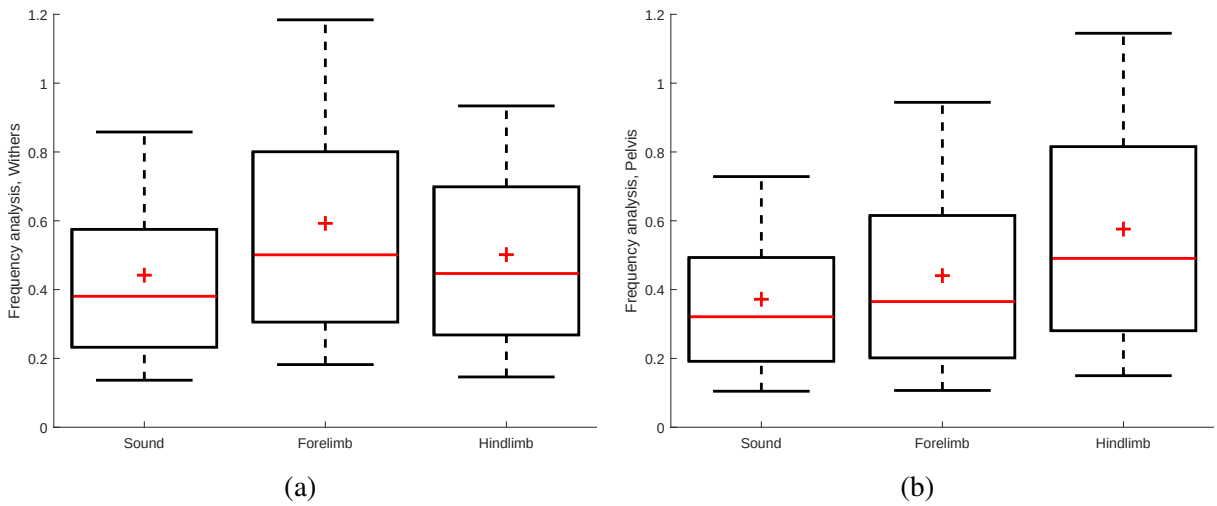

Figure 19. *(a) Box plots of the amplitude ratio ϱ_w for the withers. (b) Box plots of the amplitude ratio ϱ_p for the pelvis.*

additionally take the induction type into account in the analysis, which gives the result shown in Figure 20. It appears that it is supporting lameness that is best detected by this approach.

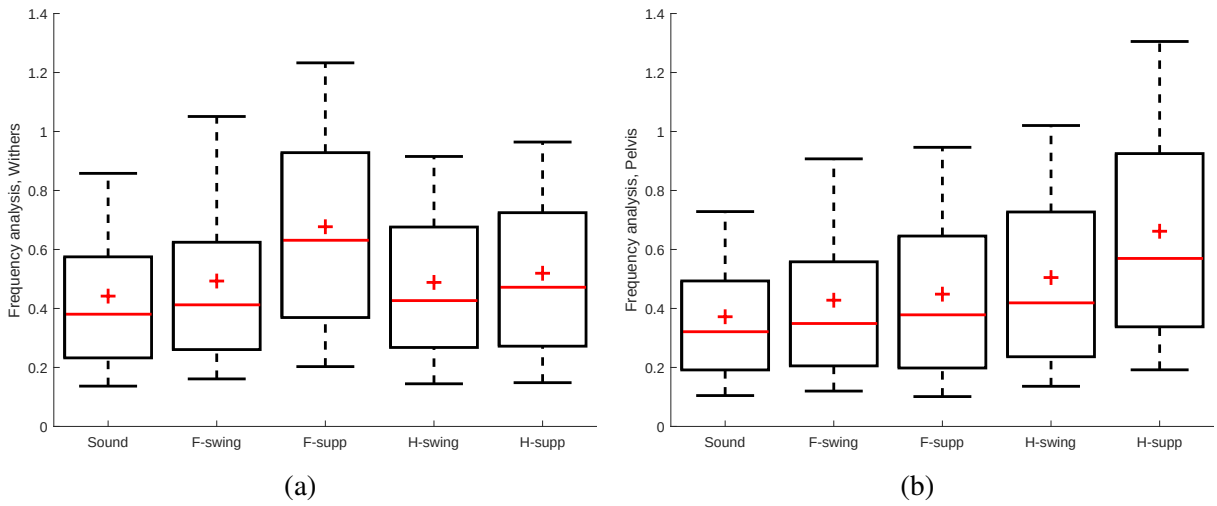

Figure 20. *(a) Box plots of the amplitude ratio ϱ_w for the withers separated by induction type. (b) Box plots of the amplitude ratio ϱ_p for the pelvis separated by induction type.*

5 DISCUSSION AND FUTURE WORK

We have in this study evaluated the feasibility of using inertial sensors, signal processing and software algorithms for lameness assessment, where the main goal has been to arrive at a more objective measure compared to what is standard in today's veterinary clinics.

Thirteen clinically sound dogs of medium size were included in the study. The study was limited to considering only trotting locomotion on straight paths indoors, simulating both common examination procedures and facilities available at most veterinary clinics. In order to have controlled experimental conditions, locomotion disturbances were induced artificially by using cotton wads at the paws and weights on the limbs. A complication with this kind of artificial lameness induction, however, is that it hard to get a consistent lameness grade during the trials since the animal often adapts to the disturbance gradually.

The results indicate that it would be feasible to use standard low cost MEMS IMUs to evaluate and assess lameness of grade 2-3 in trotting dogs, but that more work probably is needed to fine-tune and robustify the algorithms. Due to their low cost, MEMS sensors are more or less available to almost everyone today, for instance by using mobile phones with data recording apps, or by using single-board microcontrollers and microcontroller kits like Arduino, Raspberry Pi® etc.

There are many parts in the proposed movement analysis algorithm that can be improved. One obvious topic to investigate is why we get a relative high degree of asymmetry already at a low lameness grade. Another question is why the data from the withers sensor do not provide as good results as the data from the pelvis sensor. Both these problems could be related to the fact that a dog, in contrast to a horse, in general has a much more loose and flexible skin, especially in the withers region. Thus the sensors will move more and induce more disturbances when attached to a dog during locomotion. The use of home-made textile harnesses, Velcro and double adhesive tape to attach the sensors to the animals during the trials worked rather well, but it happened several times that the sensors got loose. It would therefore be desirable to come up with a more failsafe way of fastening the sensors, preferably in a way that also reduces the effect of the flexible skin.

Compared to the study by (Rhodin et al., 2017) we have in this study not yet considered the use of the head sensor to assess forelimb lameness. The reason for that is mainly the physical behavior of dogs compared to horses. A horse is typically moving more or less autonomously when locomotion exercise has been initiated, whereas a dog is more eager to please the handler and seeks eye contact. Sometimes one also has to motivate the dog to participate in the procedure by using treats, which might introduce disturbances when the dog tries to catch the treat. Another complication is the use of a leash which might affect the animal's ability to move freely.

There is of course also many aspects of the signal processing part of the work that can be enhanced. Especially the stride splitting part in the software and the algorithm that evaluates the quality and shape of the strides could be improved. Also the AHRS algorithm could obviously be improved due to the drifts in the orientation estimates which are currently present. It might be possible that the magnetometer measurements could be used if a thorough calibration routine

is carried out prior to the trials.

POPULÄRVETENSKAPLIG SAMMANFATTNING

HÄLTA eller andra rörelsestörningar är vanliga skäl till varför djurägare söker veterinärvård för sina djur. Hältan hos djuret är oftast smärtutlöst och kan bero på muskel- och/eller skelettskador, degenerativa förändringar i leder etc.

Utvärdering av hälta har traditionellt utförts genom att veterinären observerar djuret under rörelse och på så sätt bedömer om eventuella asymmetrier i rörelsemönstret föreligger. Detta är en speciellt vanlig undersökning inom hästmedicin. Ett problem är dock att bedömningen är subjektiv, dvs olika veterinärer kommer ofta till olika slutsatser. Detta har bekräftats i ett flertal publicerade studier utförda både inom hästmedicin och smådjursmedicin. Dessvärre blir situationen ännu mer utmanande när det gäller sällskapsdjur som hundar. Deras rörelser är både snabbare och mindre i magnitud jämfört med stora djur, så det kan vara svårt för det mänskliga ögat att uppfatta eventuella asymmetrier.

Datorstödd rörelseanalys med kamerabaserade eller tröghetssensorbaserade system, har blivit allt vanligare vid större hästkliniker idag som ett mer objektivt verktyg för att utvärdera rörelsestörningar. Data från djuret samlas in under under rörelse och analyseras i ett datorprogram varefter ett mått på rörelseasymmetrierna erhålls. Sådana verktyg har visat sig vara till stor nytta både vid rutinundersökningar och i mer komplicerade fall då man kan följa hur hältan förändras över tid.

Vad vi vet finns det inte något liknande kommersiellt verktyg tillgängligt för sällskapdjur såsom hundar ännu. I en nyligen genomförd studie vid SLU som utvärderade användningen av tröghetssensorer på hundar som travade på ett löpband, erhölls dock lovande resultat vid en måttlig artificiellt inducerad hälta. I denna studie utnyttjades ett kommersiellt system för hästar som hade modifierats med en speciellanpassad mjukvara. Kompletterande studier har därför ansetts önskvärda för att avgöra om denna metod kan användas under mindre kontrollerade former, t ex i ett rum eller i en korridor vid en veterinärklinik.

Syftet med detta arbete har därför varit att undersöka om det är möjligt att använda tröghetssensorer, signalbehandling och mjukvarualgoritmer för att utvärdera rörelsestörningar hos hundar under förhållanden som råder vid en helt vanlig veterinärklinik. Tröghetssensorer är numera både små, billiga och strömsnåla. De används t ex i smarta mobiltelefoner för positionering, bl a genom att mäta accelerationer och rotationshastigheter.

Studien omfattade 13 friska hundar av medelstorlek, och begränsades till att endast beakta rörelseasymmetrier vid trav på rakt spår. För att kunna garantera kontrollerade förutsättningar inducerades rörelsestörningar på konstgjord väg genom att applicera bomullsvaddar mellan tårna eller vikter på benen ovanför karpus respektive tarsus. Induktionerna anpassades så att en hältgrad 2-3 på en 5-gradig skala uppnåddes. Mätdata samlades in genom att tröghetssensorer från ett kommersiellt mätsystem fästes vid 4 positioner på hundarna; på huvudet, över manken, över bäckenet och på ett av frambenen. Dataanalys gjordes sedan offline med olika mjukvaru-

algoritmer för att utröna om eventuella rörelseasymmetrier förelåg.

Resultaten indikerar att det förefaller lovande att använda tröghetssensorer av standardtyp för att analysera rörelseasymmetrier av grad 2-3 hos hundar, men att ytterligare forskning och utveckling sannolikt krävs för att förbättra och robustifiera algoritmerna. Skillnaden mellan hästar och hundar i både beteende och fysik leder till nya utmaningar som måste hanteras. Hundar interagerar med sin förare i betydligt högre utsträckning, genom att t ex söka ögonkontakt, och deras rörelser har högre frekvens och lägre magnitud. Dessutom är huden/pälsen hos en hund generellt mer lös och flexibel, vilket innebär en utmaning när sensorerna ska fästas.

REFERENCES

W. Back and H. M. Clayton. *Equine Locomotion*. Elsevier Ltd, 2nd edition, 2013.

S. Bosch, F. Serra Bragança, M. Marin-Perianu, R. Marin-Perianu, B. van der Zwaag, J. Voskamp, W. Back, R. Van Weeren, and P. Havinga. Equimoves: A wireless networked inertial measurement system for objective examination of horse gait. *Sensors (Switzerland)*, 18(3), 2018. ISSN 14248220.

R. N. Bracewell. *The Fourier Transform and its Applications*. McGraw-Hill Higher Education, 1999.

F. Bragança, S. Bosch, J. Voskamp, M. Marin Perianu, B. Van Der Zwaag, J. Vernooij, P. Van Weeren, and W. Back. Validation of distal limb mounted inertial measurement unit sensors for stride detection in warmblood horses at walk and trot. *Equine Veterinary Journal*, 49(4), 2017. ISSN 0425-1644. URL https://biblio.ugent.be/publication/8556476.

C. E. DeCamp, S. A. Johnston, L. M. Déjardin, and S. L. Schaefer. *Brinker, Piermattei and Flo's Handbook of Small Animal Orthopedics and Fracture Repair*. Elsevier Inc, 5th edition, 2016.

B. Graf. Quaternions and dynamics. *arXiv e-prints*, art. arXiv:0811.2889, Nov. 2008.

F. Gustafsson. *Statistical Sensor Fusion*. Studentlitteratur, Lund, Sweden, 3rd edition, 2018.

G. Jenkins, N. Yang, G. Yao, and D. Duan. Automatic characterization of stride parameters in canines with a single wearable inertial sensor. *PLoS One*, 13(6), 2018. ISSN 19326203. URL http://search.proquest.com/docview/2055611037/.

R. E. Kalman. A new approach to linear filtering and prediction problems. *Journal of basic Engineering*, 82(1):35–45, 1960.

P. Kasebzadeh and F. Gustafsson. Gait cycle modeling. Personal communication, October 2018. Dept of Electrical Engineering, Linköping University, Sweden.

K. G. Keegan, Y. Yonezawa, P. F. Pai, D. A. Wilson, and J. Kramer. Evaluation of a sensor-based system of motion analysis for detection and quantification of forelimb and hind limb lameness in horses. *American journal of veterinary research*, 65(5), 2004. ISSN 0002-9645.

K. G. Keegan, E. V. Dent, D. A. Wilson, J. Janicek, J. Kramer, A. Lacarrubba, D. M. Walsh, M. W. Cassells, T. M. Esther, P. Schiltz, K. E. Frees, C. L. Wilhite, J. M. Clark, C. C. Pollitt, R. Shaw, and T. Norris. Repeatability of subjective evaluation of lameness in horses. *Equine Veterinary Journal*, 42(2):92–97, 2010. ISSN 0425-1644.

K. G. Keegan, J. Kramer, Y. Yonezawa, H. Maki, P. F. Pai, E. V. Dent, T. E. Kellerman, D. A. Wilson, and S. K. Reed. Assessment of repeatability of a wireless, inertial sensor-based lameness evaluation system for horses. *American journal of veterinary research*, 72(9), 2011. ISSN 1943-5681.

J. B. Kuipers. Quaternions and Rotation Sequences. In *Proceedings of the International Conference on Geometry, Integrability and Quantization*, pages 127–143. Coral Press Scientific Publishing, 2000. ISBN 9780691102986. doi: 10.2307/3909157.

C. Ladha, J. O'sullivan, Z. Belshaw, and L. Asher. Gaitkeeper: A system for measuring ca-

nine gait. *Sensors*, 17(2), 2017. ISSN 1424-8220. URL https://doaj.org/article/233b26aa5b744f8fa1b9d8e136fe7302.

MathWorks. *MATLAB version 9.5.0.944444 (R2018b)*. The MathWorks Inc., Natick, Massachusetts, USA, 2018.

E. Olsen, P. H. Andersen, and T. Pfau. Accuracy and precision of equine gait event detection during walking with limb and trunk mounted inertial sensors. *Sensors (Basel, Switzerland)*, 12(6), 2012. ISSN 1424-8220.

T. Pfau, T. H. Witte, and A. M. Wilson. A method for deriving displacement data during cyclical movement using an inertial sensor. *The Journal of experimental biology*, 208(Pt 13), 2005. ISSN 0022-0949.

T. Pfau, S. D. Starke, S. Tröster, and L. Roepstorff. Estimation of vertical tuber coxae movement in the horse from a single inertial measurement unit. *The Veterinary Journal*, 198(2):498–503, 2013. ISSN 1090-0233.

M. Rhodin, A. Bergh, P. Gustås, and C. Gómez Álvarez. Inertial sensor-based system for lameness detection in trotting dogs with induced lameness. *The Veterinary Journal*, 222(C): 54–59, 2017. ISSN 1090-0233.

S. D. Starke, E. Willems, S. A. May, and T. Pfau. Vertical head and trunk movement adaptations of sound horses trotting in a circle on a hard surface. *Veterinary journal (London, England : 1997)*, 193(1), 2012. ISSN 1532-2971.

A. S. Waxman, D. A. Robinson, R. B. Evans, D. A. Hulse, J. F. Innes, and M. G. Conzemius. Relationship between objective and subjective assessment of limb function in normal dogs with an experimentally induced lameness. *Veterinary Surgery*, 37(3):241–246, 2008. doi: 10.1111/j.1532-950X.2008.00372.x. URL https://onlinelibrary.wiley.com/doi/abs/10.1111/j.1532-950X.2008.00372.x.

Wikipedia contributors. Inertial measurement unit — Wikipedia, the free encyclopedia. https://en.wikipedia.org/w/index.php?title=Inertial_measurement_unit&oldid=864934959, 2018. [Online; accessed 31-October-2018].

R. Zanetti, M. Majji, R. H. Bishop, and D. Mortari. Norm-constrained kalman filtering. In *Proceedings of the 2006 AIAA/AAS Astrodynamics Specialist Conference*, number 2006-6161 in AIAA, 2006.

Appendices

A NUMERIC INTEGRATION

A common method for approximating the definite integral

$$s = \int f(t)\,dt \tag{17}$$

numerically in the time domain, is to utilize the *trapezoidal rule*. If we assume that the data is sampled with sample interval T_s yielding N samples, and we use the notation $f[k] = f(kT_s)$, we have that

$$s[N] = \int_{T_s}^{NT_s} f(t)\,dt \approx T_s \sum_{k=1}^{N} \frac{f[k] + f[k-1]}{2}. \tag{18}$$

Here we assume that $f[0] = 0$. For double integrals, the rule (18) is applied twice. In practice, however, it is often required to pre-process the data, such as filtering and/or removals of mean values, in order to avoid cumulating errors, so-called *drifts*.

Integration can also be performed in the frequency domain. Let

$$F[n] = \sum_{k=1}^{N} f[k] \cdot e^{-i\Omega_n k}, \quad n = 1, \ldots, N \tag{19}$$

denote the discrete Fourier transform (DFT) of $f[k]$, see Bracewell (1999), with $i = \sqrt{-1}$ and

$$\Omega_n = \frac{2\pi n}{N}. \tag{20}$$

Then it can be shown that integration in the time domain is the same as multiplying $F[n]$ with $T_s/(i\Omega_n)$ in the frequency domain, i.e.,

$$S[n] = \frac{T_s}{i\Omega_n} F[n]. \tag{21}$$

By taking the inverse discrete Fourier transform (IDFT) of $S[n]$,

$$s[k] = \sum_{n=1}^{N} S[n] \cdot e^{i\Omega_n k}, \tag{22}$$

we thus obtain the integral in the time domain. A double integral can be computed by multiplying $F[n]$ with $-T_s^2/\Omega_n^2$. In implementations we will use the fast Fourier transform (FFT) instead of DFT.

B AHRS

A system that estimates the orientation or attitude of an object relative the earth frame is called an *attitude and heading reference system* (AHRS). Different approaches for AHRSs have been thoroughly studied within the fields of avionics and robotics. I have in this work investigated the use of an Extended Kalman filter (EKF) based on quaternions.

B.1 Kalman Filtering

The concept and theory of *Kalman filtering* is well matured and has been thoroughly analyzed and investigated since its introduction in the 1960s (Kalman, 1960). The Kalman filter assumes that measured data is thought to has been generated by a linear dynamic state-space model according to

$$x[k+1] = F_k x[k] + G_k u[k] + v[k], \tag{23a}$$

$$y[k] = H_k x[k] + e[k]. \tag{23b}$$

where $x[k]$ is the system state, $u[k]$ is the input, $y[k]$ is the output, and $v[k]$ and $e[k]$ are process and measurement noise respectively. Using observations $u[k]$ and $y[k]$ from the system (23), the goal is then to estimate the state vector $x[k]$. A straightforward approach to estimate the states is to utilize a *state observer*, i.e.,

$$\hat{x}[k+1] = F_k \hat{x}[k] + G_k u[k] + K_k \left(y[k] - H_k \hat{x}[k]\right). \tag{24}$$

where K_k is the *observer gain*. The Kalman filter selects the optimal observer gain given knowledge of the statistical properties of $v[k]$ and $e[k]$. More specifically, the recursive Kalman filter algorithm can be formulated as

$$K_k = P_{k|k-1} H_k^T \left(H_k P_{k|k-1} H_k^T + R_k\right)^{-1}, \tag{25a}$$

$$\hat{x}[k|k] = \hat{x}[k|k-1] + K_k \left(y[k] - H_k \hat{x}[k|k-1]\right), \tag{25b}$$

$$P_{k|k} = P_{k|k-1} - K_k H_k P_{k|k-1} \tag{25c}$$

$$\hat{x}[k+1|k] = F_k \hat{x}[k|k] + G_k u[k], \tag{26a}$$

$$P_{k+1|k} = F_k P_{k|k} F_k^T + Q_k \tag{26b}$$

where R_k and Q_k are the covariance matrices of $e[k]$ and $v[k]$ respectively. Here (25) is referred to as the *measurement update* (or update step) since it incorporates the measurements $y[k]$ in the recursion, and (26) is called the *time update* (or prediction step).

If the system description instead is nonlinear in $x[k]$ and $u[k]$, i.e.,

$$x[k+1] = f(x[k], u[k]) + v[k], \tag{27a}$$

$$y[k] = h(x[k]) + e[k], \tag{27b}$$

for some nonlinear functions $f(\cdot)$ and $h(\cdot)$, a common approximation is to linearize these functions around the current state estimate. Then one ends up with the so-called *extended Kalman filter* (EKF) where F_k, G_k and H_k in (25) and (26) are replaced with the Jacobians of $f(\cdot)$ and $h(\cdot)$ evaluated at the current state estimate. That is,

$$F_k \approx \left.\frac{\partial f(x,u)}{\partial x}\right|_{x=\hat{x}[k|k]}, \tag{28a}$$

$$G_k \approx \left.\frac{\partial f(x,u)}{\partial u}\right|_{u=u[k]}, \tag{28b}$$

$$H_k \approx \left.\frac{\partial h(x)}{\partial x}\right|_{x=\hat{x}[k|k]}. \tag{28c}$$

B.2 Attitude and Heading

Describing the orientation of an object in 3D space can be done in several ways where Euler angles or rotation matrices are commonly used approaches.

B.2.1 Euler Angles

Euler discovered that any orientation can be achieved by applying three elementary rotations around the coordinate axes. Let ϕ, θ and ψ denote the Euler angles, i.e., the rotation angles around the x, y and z axes respectively. Then it can be shown that an arbitrary rotation can be expressed as

$$\begin{aligned}
\begin{pmatrix} x' \\ y' \\ z' \end{pmatrix} &= R \begin{pmatrix} x \\ y \\ z \end{pmatrix} = R_x(\phi) R_y(\theta) R_z(\psi) \begin{pmatrix} x \\ y \\ z \end{pmatrix} \\
&= \begin{pmatrix} 1 & 0 & 0 \\ 0 & \cos\phi & -\sin\phi \\ 0 & \sin\phi & \cos\phi \end{pmatrix} \begin{pmatrix} \cos\theta & 0 & \sin\theta \\ 0 & 1 & 0 \\ -\sin\theta & 0 & \cos\theta \end{pmatrix} \begin{pmatrix} \cos\psi & -\sin\psi & 0 \\ \sin\psi & \cos\psi & 0 \\ 0 & 0 & 1 \end{pmatrix} \begin{pmatrix} x \\ y \\ z \end{pmatrix} \\
&= \begin{pmatrix} \cos\theta\cos\psi & \cos\theta\sin\psi & -\sin\theta \\ \sin\phi\sin\theta\cos\psi - \cos\phi\sin\psi & \sin\phi\sin\theta\sin\psi + \cos\phi\cos\psi & \sin\phi\cos\theta \\ \cos\phi\sin\theta\cos\psi + \sin\phi\sin\psi & \cos\phi\sin\theta\sin\psi - \sin\phi\cos\psi & \cos\phi\cos\theta \end{pmatrix} \begin{pmatrix} x \\ y \\ z \end{pmatrix}
\end{aligned} \tag{29}$$

where R is an orthogonal rotation matrix satisfying $R^{-1} = R^T$. When the object is rotating in 3D space, the Euler angles change according to

$$\begin{pmatrix} \omega_x \\ \omega_y \\ \omega_z \end{pmatrix} = \begin{pmatrix} \frac{d}{dt}\phi \\ 0 \\ 0 \end{pmatrix} + R_x(\phi) \begin{pmatrix} 0 \\ \frac{d}{dt}\theta \\ 0 \end{pmatrix} + R_x(\phi) R_y(\theta) \begin{pmatrix} 0 \\ 0 \\ \frac{d}{dt}\psi \end{pmatrix}. \tag{30}$$

The dynamics of the Euler angles can be derived from this as

$$\frac{d}{dt} \begin{pmatrix} \phi \\ \psi \\ \theta \end{pmatrix} = \begin{pmatrix} 1 & \sin\phi\tan\theta & \cos\phi\tan\theta \\ 0 & \cos\phi & -\sin\phi \\ 0 & \frac{\sin\phi}{\cos\theta} & \frac{\cos\phi}{\cos\theta} \end{pmatrix} \begin{pmatrix} \omega_x \\ \omega_y \\ \omega_z \end{pmatrix}. \tag{31}$$

The matrix in (31) becomes singular when $\theta \pm \pi/2 + n \cdot \pi$ which can cause problems in a Kalman filter context.

B.2.2 Quaternions

A better and more numerically stable approach is to use *quaternions*, which can be interpreted as an extension of the concept of complex numbers, see for instance (Kuipers, 2000). A quaternion consists of a real part and three imaginary parts usually denoted as

$$q = q_w + i q_x + j q_y + k q_z, \tag{32}$$

where q_w is the real part, and q_x, q_y and q_z are the imaginary parts. It is common to represent a quaternion as a vector (i.e., column matrix) such that

$$q = \left(q_w,\ q_x,\ q_y,\ q_z\right)^T. \tag{33}$$

A quaternion can be used to describe a rotation an angle α around a vector

$$\omega = \left(\omega_x,\ \omega_y,\ \omega_z\right)^T \tag{34}$$

in 3D space as

$$q = \begin{pmatrix} \cos\frac{\alpha}{2} \\ \sin\frac{\alpha}{2}\cdot\omega \end{pmatrix}. \tag{35}$$

This provided the vector q has *unit length*, i.e., $|q|^2 = q_w^2 + q_x^2 + q_y^2 + q_z^2 = 1$. The quaternion can be converted to a rotation matrix according to

$$R = R(q) = \begin{pmatrix} q_w^2 + q_x^2 - q_y^2 - q_z^2 & 2(q_x q_y - q_w q_z) & 2(q_w q_y + q_x q_z) \\ 2(q_x q_y + q_w q_z) & q_w^2 - q_x^2 + q_y^2 - q_z^2 & 2(q_y q_z - q_w q_x) \\ 2(q_x q_z - q_w q_y) & 2(q_y q_z + q_w q_x) & q_w^2 - q_x^2 - q_y^2 + q_z^2 \end{pmatrix}. \tag{36}$$

If ω is time-dependent (i.e., $\omega = \omega(t)$), it can be shown, see for instance (Graf, 2008), that the dynamic behavior of the quaternion is governed by

$$\frac{d}{dt}q(t) = \frac{1}{2}\begin{pmatrix} 0 \\ \omega(t) \end{pmatrix} \otimes q(t). \tag{37}$$

where $\otimes$ denotes Hamilton (quaternion) product. One can show that the Hamilton product can be expressed as a matrix multiplication, so that

$$\frac{d}{dt}q(t) = \frac{1}{2}S(\omega(t))q(t) = \frac{1}{2}\bar{S}(q(t))\omega(t), \tag{38}$$

with

$$S(\omega) = \begin{pmatrix} 0 & -\omega_x & -\omega_y & -\omega_z \\ \omega_x & 0 & -\omega_z & \omega_y \\ \omega_y & \omega_z & 0 & -\omega_x \\ \omega_z & -\omega_y & \omega_x & 0 \end{pmatrix} \quad \text{and} \quad \bar{S}(q) = \begin{pmatrix} -q_x & -q_y & -q_z \\ q_w & q_z & -q_y \\ -q_z & q_w & q_x \\ q_y & -q_x & q_w \end{pmatrix}. \tag{39}$$

Here we use the same notation as Gustafsson (2018).

B.3 A Quaternion-based EKF

In order to use the dynamic relation (38) in a Kalman filter (i.e., being able to to express it in a form similar to equations (23) or (27)), we have to solve the differential equation (38) on the sample interval $[kT_s,\ (k+1)T_s]$ assuming $\omega[k]$ is constant. We then get

$$\begin{aligned} q[k+1] &= e^{\frac{1}{2}S(\omega[k])T_s}q[k] \\ &= \left(\cos\frac{|\omega[k]|\,T_s}{2}I + \frac{T_s}{2}\frac{\sin\frac{|\omega[k]|T_s}{2}}{\frac{|\omega[k]|T_s}{2}}S(\omega[k])\right)q[k] \\ &\approx \left(I + \frac{T_s}{2}S(\omega[k])\right)q[k]. \end{aligned} \tag{40}$$

where I denotes the identity matrix, see for instance (Gustafsson, 2018). A complication is that we are not measuring the true angular velocity via a MEMS gyroscope, rather a sum of the true angular velocity $\omega^0[k]$, the gyro bias $b^g[k]$, and measurement noise $v^\omega[k]$,

$$\omega[k] = \begin{pmatrix} \omega_x[k] \\ \omega_y[k] \\ \omega_z[k] \end{pmatrix} = \omega^0[k] + b^g[k] - v^\omega[k] = \begin{pmatrix} \omega_x^0[k] + b_x^g[k] - v_x^\omega[k] \\ \omega_y^0[k] + b_y^g[k] - v_y^\omega[k] \\ \omega_z^0[k] + b_z^g[k] - v_z^\omega[k] \end{pmatrix}. \tag{41}$$

Thus

$$\begin{aligned} q[k+1] &\approx \left(I + \frac{T_s}{2} S\left(\omega[k] - b^g[k] + v^\omega[k]\right) \right) q[k] \\ &= \left(I + \frac{T_s}{2} S\left(\omega[k]\right) \right) q[k] - \frac{T_s}{2} \bar{S}(q[k]) b^g[k] + \frac{T_s}{2} \bar{S}(q[k]) v^\omega[k]. \end{aligned} \tag{42}$$

We chose to model the dynamics of the gyro bias as a *random walk*, that is,

$$b^g[k+1] = b^g[k] + v^b[k], \tag{43}$$

where $v^b[k]$ is normally distributed noise with zero mean. In order to use the models (42) and (43) in the EKF framework we use the measured angle velocities as input vector,

$$u[k] = \left(\omega_x[k],\ \omega_y[k],\ \omega_z[k]\right)^T, \tag{44}$$

the measured accelerations as output vector,

$$y[k] = \left(a_x[k],\ a_y[k],\ a_z[k]\right)^T, \tag{45}$$

and the quaternion and gyro offsets as state vector,

$$x[k] = \left(q_w[k],\ q_x[k],\ q_y[k],\ q_z[k],\ b_x^g[k],\ b_y^g[k],\ b_z^g[k]\right)^T. \tag{46}$$

The system dynamics can then be summarized in matrix form as

$$x[k+1] = \underbrace{\begin{pmatrix} I + \frac{T_s}{2} S(\omega[k]) & -\frac{T_s}{2} \bar{S}(q[k]) \\ 0 & I \end{pmatrix}}_{F_k} x[k] + \underbrace{\begin{pmatrix} \frac{T_s}{2} \bar{S}(q[k]) & 0 \\ 0 & T_s I \end{pmatrix} \begin{pmatrix} v^\omega[k] \\ v^b[k] \end{pmatrix}}_{\tilde{v}_k}. \tag{47}$$

The system outputs (45) relate to the state vector (46) as

$$y[k] = R(q[k])^T \left(a^0[k] + g_v\right) + e[k] = h(q[k]) + e[k], \tag{48}$$

where the $R(q)^T$ is the transpose of the rotation matrix in (36) which rotates from the earth frame to the IMU frame, $a^0[k]$ is the acceleration vector of the IMU in the earth frame, $g_v = (0,\ 0,\ -1)^T$ is the gravity vector in the earth frame, and $e[k]$ is measurement noise. The acceleration vector $a^0[k]$ is not known though, so we have to assume $a^0[k] = 0$. The relation (48) is obviously nonlinear in $q[k]$ according to (36), so we have to linearize and compute the Jacobian of $h(\cdot)$,

$$H_k \approx \left. \frac{\partial h(x)}{\partial x} \right|_{x=\hat{q}[k]}. \tag{49}$$

Note that we have to ensure the unit length constraint when using the state transition model (47) in an EKF so that $\hat{q}_w^2[k] + \hat{q}_x^2[k] + \hat{q}_y^2[k] + \hat{q}_z^2[k] = 1$. This can be achieved by means of normalization, see (Zanetti et al., 2006).

By combining (29) and (36) the estimates of the Euler angles become

$$\begin{pmatrix} \hat{\phi}[k] \\ \hat{\theta}[k] \\ \hat{\psi}[k] \end{pmatrix} = \begin{pmatrix} \arctan \frac{2\left(\hat{q}_y[k]\hat{q}_z[k] - \hat{q}_w[k]\hat{q}_x[k]\right)}{\hat{q}_w^2[k] - \hat{q}_x^2[k] - \hat{q}_y^2[k] + \hat{q}_z^2[k]} \\ \arcsin\left(2\left(\hat{q}_w[k]\hat{q}_y[k] + \hat{q}_x[k]\hat{q}_z[k]\right)\right) \\ \arctan \frac{2\left(\hat{q}_x[k]\hat{q}_y[k] - \hat{q}_w[k]\hat{q}_z[k]\right)}{\hat{q}_w^2[k] + \hat{q}_x^2[k] - \hat{q}_y^2[k] - \hat{q}_z^2[k]} \end{pmatrix} \tag{50}$$

The measured accelerations (in the IMU frame) can be rotated to the earth frame using

$$a_e[k] = R\left(\hat{q}[k]\right) a[k] - g_v, \tag{51}$$

or by using the quaternion directly

$$\begin{pmatrix} 0 \\ a_e[k] \end{pmatrix} = \hat{q}[k] \otimes \begin{pmatrix} 0 \\ a[k] \end{pmatrix} \otimes \hat{q}^*[k] - \begin{pmatrix} 0 \\ g_v \end{pmatrix}, \tag{52}$$

where q^* is the inverse/conjugate of the quaternion.

So far we have only considered a single extended Kalman filter for one IMU. If we want to estimate the states for several IMUs in parallel we can just stack them in the filter. However, they will then be completely independent.

The yaw estimates can be stabilized utilizing the special condition that the dogs are running on straight paths with 180° turns in the ends during the trials. Consider the Euler angles in equation (50). By dropping the time indices and the "hats" for ease of notation, we have that the yaw ψ is given by

$$\psi = \arctan \frac{2\left(q_x q_y - q_w q_z\right)}{q_w^2 + q_x^2 - q_y^2 - q_z^2}. \tag{53}$$

The yaw is thus 0° or 180° (+ $n \cdot 360°$) when the numerator in (53) equals zero. We can take advantage of this knowledge in the filter by adding a virtual measurement in the filter output in (48)

$$0 = h_1(q) = \left(q_x q_y - q_w q_z\right)^2. \tag{54}$$

Of course we need also to extend the H_k matrix in (49) with the partial derivatives of h_1 with respect to q.

Another idea is to try to stabilize the yaw estimate from the IMUs at the pelvis and withers by adding dependencies between them. Given the two quaternions q^p (pelvis) and q^w (withers) we can again extend the filter outputs in (48) with the squared differences of the numerators and denominators in (53)

$$0 = h_2(q^p, q^w) = \left(q_x^p q_y^p - q_w^p q_z^p - q_x^w q_y^w + q_w^w q_z^w\right)^2, \tag{55a}$$

$$\begin{aligned} 0 = h_3(q^p, q^w) = \big((q_w^p)^2 + (q_x^p)^2 - (q_y^p)^2 - (q_z^p)^2 \\ -(q_w^w)^2 - (q_x^w)^2 + (q_y^w)^2 + (q_z^w)^2\big)^2, \end{aligned} \tag{55b}$$

thus to some extent forcing them, and the corresponding yaw estimates, to move towards the same values. Also here we need to extend the H_k matrix in (49) with the partial derivatives of h_2 and h_3 with respect to q^p and q^w.